DESIGN AND OPTIMISATION OF A LIQUID METAL SPALLATION TARGET FOR THE ENERGY AMPLIFIER PROTOTYPE

L. Maciocco, V. Bellucci, S. Buono, G. Fotia,
V. Moreau, M. Mulas, G. Siddi, L. Sorrentino

CRS4 Research Center
Via N. Sauro, 10
I-90123 - Cagliari (Italy)
+39 70 2796-334

ABSTRACT

The thermo-fluid-dynamic and structural analysis of the spallation target for the Energy Amplifier [1] (EA) is presented. The sensitivity of the system to the geometrical and physical parameters has been analysed through extensive numerical thermo-fluid-dynamic (TFD) simulations performed with the Star-CD commercial code [2]. Starting from the results obtained with the fluid dynamic analysis, a linear structural analysis of the window-pipe system has been performed with the MSC/Nastran finite-elements code [3].

The result of this work is a set of design guidelines for the final sizing of the target.

I. INTRODUCTION

The target represents one of the main technological problems related not only to the design of the EAP, but to all High Power Spallation Sources (HPSS) currently under study or in construction world-wide [4, 5]. The most common target configurations adopted in HPSS designs include a beam window which separates the internal vacuum of the beam pipe from the molten metal target. Given the fact that the primary cooling loop of the EAP is made of lead-bismuth eutectic (LBE), we considered the same material for the beam target.

The most important problems related to all target designs are target cooling, high energy neutron radiation damage and liquid metal corrosion. Configurations using a beam window have the additional problems of the beam window cooling and the radiation damage induced in the beam window material, which is of a slight different nature of the one induced in the other structures, since the window is exposed not only to back scattered high energy neutrons, but also to the high energy proton flux. While steels might be suitable candidates for low power applications [4, 5] as is the case of the EAP, refractory alloys or more advanced materials are mandatory for high power applications [6, 7].

The cooling of the EAP target is effected by the natural circulation of the liquid Pb-Bi, which has the double function of removing the heat produced in the spallation process and of cooling the beam window. The efficiency of the natural circulation depends on the target height (which is related to the dimensions of the primary circuit of the EAP) and on the fluid dynamic design of the coolant circuit. In the present work a target height of about 6 m is considered. The study and optimization of the target cooling flow is presented in the following.

II. DESCRIPTION

A. Geometrical Description

The target is an axisymmetric device (Fig. 1) consisting of a vertical pipe ("beam pipe") closed at the bottom by an hemisphere of variable thickness ("window"); the beam pipe is enclosed in a vertical coaxial cylinder with an hemispherical bottom ("container"). The region between the beam pipe and the container is filled with the spallation-cooling fluid (coolant). The region inside the beam pipe is filled with air at very low pressure (void). The flow of the coolant is guided by a coaxial cylinder laying between the beam pipe and the container ("flow guide") which separates the hot rising flow coming from the spallation region from the cold downcoming flow cooled in the heat exchanger, which is positioned on the top of the downcoming duct. In the spallation region the flow guide is shaped like a funnel in order to enhance the cooling of the window. The funnel is made of a converging duct ("inducer"), which turns the flow from the downcoming duct into the short pipe ("funnel") where the spallation takes place. The funnel and the rising duct are connected by a divergent duct ("connector").

The beam pipe (and window) diameter has been

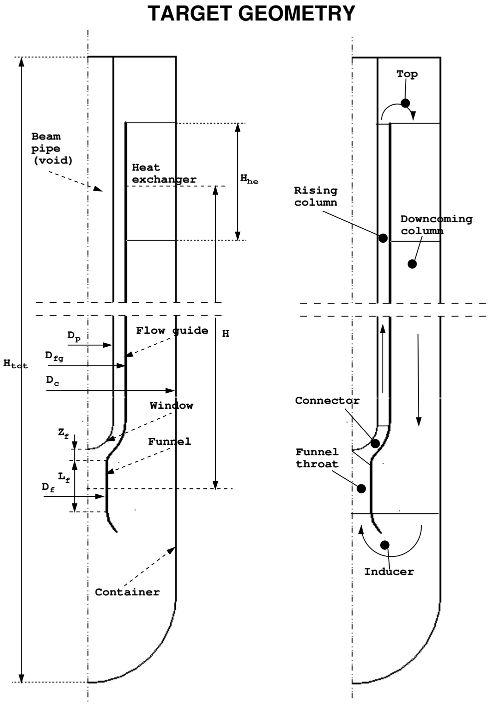

Figure 1: geometry of the model and description of the coolant circuit.

assumed to be 200 mm, in order to allow a correct defocusing of the beam spot to prevent localised high power density in the target materials. The external surface of the window is an hemisphere while the internal surface is an ellipsoid, so that the window thickness varies from a minimum of 1.5 mm in the beam axis to a maximum of 3 mm in the junction with the beam pipe; this was done in order to reduce the thickness as much as possible in the zone where proton irradiation is higher, keeping a sufficient structural resistance.

The beam pipe and the container are all made of HT-9 steel. In general the flow guide is made of two layers of steel with a layer of insulating material (Zirconium oxide) between them. Both cases with and without insulation and with different flow guide thickness were considered (the results are not reported here) leading to the conclusion that insulation is not strictly necessary.

B. Physical Description

1. The window cooling mechanism. Owing to the interactions between the proton beam and the window material, there is an intense heat generation inside the window (order $10^2\ W/cm^3/mA$), which is especially concentrated in the window center. Neglecting the radiation through the beam pipe vacuum region, this power must be entirely removed by the Pb-Bi flow, whose temperature is previously increased inside the funnel by the heat source $\dot{Q}_c$ generated in the spallation process. As described later (see Fig. 5) the power released in the Pb-Bi is more intense in proximity of the window center; this leads to a highly non uniform temperature distribution in the flow (an example of the temperature and velocity field in the funnel is shown in Fig. 2).

The balance between the power released inside the window and the heat transferred from the window to the coolant can be written as

$$\dot{Q}_w = A_w \overline{h}_c (\overline{T}_w - \overline{T}_{c,w}) \tag{1}$$

where $\dot{Q}_w$ is the heat released inside the window (in W), A_w is the area of the external surface of the window, $\overline{h}_c$ is the mean convective heat exchange coefficient, $\overline{T}_w$ is the mean window temperature and $\overline{T}_{c,w}$ is the mean temperature of the window cooling flow. Owing to the non uniform temperature distribution in the coolant, giving an expression for $\overline{T}_{c,w}$ is extremely difficult. It could be defined as the mean temperature increase due to the power $\dot{Q}_c$ released in the fluid:

$$\overline{T}_{c,w} = \overline{T}_{c,b} + \frac{\dot{Q}_c}{C_p\, \dot{m}} \tag{2}$$

where $\overline{T}_{c,b}$ is the mean temperature of the coolant incoming in the funnel (measured in the region at the bottom of the target), $\dot{m}$ the mass flow rate and C_p the specific heat; however this definition does not take into account that the central flow streams, i.e. the streams close to the axis, which cross the region where the heat release in the Pb-Bi is more intense, are the most effective for the window cooling. Following Eq.2, $\overline{T}_{c,w}$ would remain constant when varying the flow velocity in the funnel with constant mass flow rate, while actually the temperature of the central streams would change. For example reducing the funnel diameter while keeping constant the mass flow rate would lead to an increase of the flow velocity in the funnel resulting in a lower heating of the central streams and therefore to a better cooling of the window[a] (this effect is not caught using Eq.(2), which gives the same value for $\overline{T}_{c,w}$). This problem can be by-passed writing Eq.(1) as

$$\dot{Q}_w = A_w \overline{h}'_c (\overline{T}_w - \overline{T}_{c,b}) \tag{3}$$

In this case the convective heat exchange coefficient $\overline{h}'_c$ takes also into account the heating mechanism of the Pb-Bi through the funnel. However the value of $\overline{h}'_c$ is not comparable with the heat exchange coefficient for cases where the cooling flow has a uniform temperature.

[a]Actually the better cooling of the window is due both to the lower heating of the coolant and to the increase of the convective coefficient $\overline{h}_c$. However the former mechanism is much more effective than the second one.

A mean Nusselt number for the window can be defined on the basis of $\overline{h}_c'$ as

$$Nu_w = \frac{\overline{h}_c'\,D_w}{k} \tag{4}$$

where D_w is the window diameter and k is the thermal conductivity of the Pb-Bi. This Nusselt number is a function of the characteristics of the flow in the funnel; in particular it depends on the efficiency of the heat exchange between the window and the coolant and on the temperature distribution in the window cooling flow.

There are two mechanisms governing the flow in the funnel: the forced convection pumped by the chimney effect[b] and the local natural convection in the funnel region caused by the transversal temperature gradients. The former mechanism can be described by the funnel Reynolds number

$$Re_f = \frac{\rho\,\overline{v}_f\,D_f}{\mu} = \frac{1}{\mu}\frac{4\,\dot{m}}{\pi\,D_f^2}D_f = \frac{4}{\pi\,\mu}\frac{\dot{m}}{D_f} \tag{5}$$

where $\overline{v}_f$ is the mean velocity in the funnel. The local natural convection has the effect of increasing the velocity of the hottest streams (close to the axis) with a corresponding decrease of the velocity near the funnel walls, hence improving the window cooling. The magnitude of this mechanism can be represented by the funnel Grashof number

$$Gr_f = \frac{g\beta}{\nu^2}\overline{\Delta T}_r L_f^3 \tag{6}$$

where $\overline{\Delta T}_r$ is the temperature difference between the positions at $r = 0$ and $r = D_f/2$ averaged along the funnel[c] and β is the Pb-Bi volumetric expansion coefficient. A qualitative indication of the importance of the buoyancy mechanism with respect to the forced convection is given by the ratio Gr/Re^2. For the cases analysed here this ratio ranges from 0.02 to 0.05: so the local natural convection has a slight enhancing effect on the window cooling.

We can conclude that the convective heat exchange coefficient $\overline{h}_c$ [defined in Eq.(1)] is just a function of Re_f, while $\overline{h}_c'$ is a function of Re_f and of $\overline{T}_{c,w}$, i.e. of the temperature distribution in the coolant. Given the heat source distribution, $T_{c,w}$ is a function of $\dot{m}$ and D_f; hence, considering Eq.(5), we can write

$$Nu_w = Nu_w\,(\dot{m}, D_f) \tag{7}$$

[b] Although the flow in the target is driven by natural convection, from the point of view of the funnel it is a forced flow; in fact it would be indifferent for the flow in the funnel if the same mass flow rate were obtained with natural circulation or with pumps.

[c] The temperature gradients in the radial direction are generated by the non-uniform distribution of the heat source in the coolant and depend on the velocity field in the funnel, i.e. on Re_f, D_f and Gr_f itself.

where the function $Nu_w(\dot{m}, D_f)$ grows while increasing $\dot{m}$ and diminishing D_f.

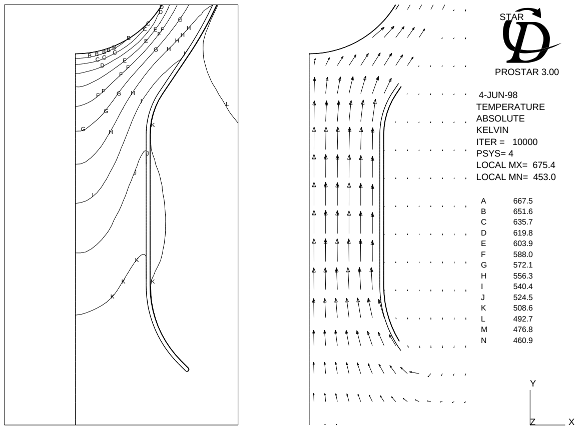

Figure 2: an example of the temperature and velocity field in the funnel.

2. The chimney effect. The one-dimensional expression for the pumping pressure generated by the chimney effect is given by

$$\Delta p = \rho\,g\,\beta\,H\,\overline{\Delta T} \tag{8}$$

where $\overline{\Delta T}$ is the difference between the mean temperatures of the rising and downcoming columns. $\overline{\Delta T}$ is the result of the heating across the spallation region and the heat $\dot{Q}_{u-d}$ exchanged between the two columns across the flow guide:

$$\overline{\Delta T} = \frac{\dot{Q}_c - \dot{Q}_{u-d}}{C_p\,\dot{m}} \tag{9}$$

where $\dot{Q}_{u-d}$ depends on the flow guide thermal resistance and on the temperatures and velocities of the rising and downcoming flows. Using Eq.(9), for a given target height H and a given power $\dot{Q}_c$ and neglecting for the sake of simplicity $\dot{Q}_{u-d}$, Eq.(8) can be written as

$$\Delta p = \frac{c_1}{\dot{m}} \tag{10}$$

where

$$c_1 = \frac{\rho\,g\,\beta\,H\,\dot{Q}_c}{C_p}$$

is a constant. Eq.(10) is an hyperbola which describes the pumping performance of the chimney effect as a function of the mass flow rate.

The dissipation losses in the circuit are given by the distributed losses in the rising and downcoming ducts plus the sum of the local losses (in the inducer, in the funnel, in the connector and in the heat exchanger):

$$\Delta p_{diss} = \Delta p_u + \Delta p_d + \sum \Delta p_{c,i} \tag{11}$$

As a first approximation the total losses in the circuit can be expressed as

$$\Delta p_{diss} = c_2 \, \dot{m}^2 \tag{12}$$

where c_2 is a constant related to the geometrical characteristics of the circuit. Eq.(12) defines the characteristic curve of the circuit.

Then, for a given target configuration and a given beam power, the operation mass flow rate is determined by the crossing point between the characteristic curves defined by Eqs. (10) and (12) (see Fig. 3). Hence dissipation losses in the circuit should be reduced as much as possible in order to maximise the mass flow rate and then maximise the heat exchange in the window [Eq.(7)].

The distributed losses in the rising and downcoming columns depend on the flow guide diameter D_{fg}. The local pressure losses in the connector, given a design criteria[d], depend on D_{fg} and on D_f while the losses in the inducer can be reduced with a suitable fluid dynamic design. In conclusion the pressure losses in the circuit depend mainly on the funnel diameter D_f and on the flow guide diameter D_{fg}.

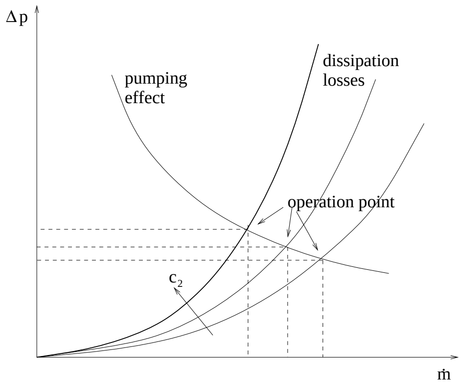

Figure 3: Characteristic curves of the natural circulation pump and of the pressure losses in the target circuit.

The effect of the heat transfer across the flow guide is to reduce the temperature difference between the rising and downcoming columns, therefore reducing the pumping efficiency of the chimney effect. In addiction it increases the temperature of the window cooling flow. This effect could be not negligible on the window temperatures and it should be taken into account.

III. THE NUMERICAL MODEL

A. Thermo-Fluid-Dynamic Analysis

The Star-CD commercial code [2] was used for the simulation of the turbulent incompressible flow of the Pb-Bi. The equations for the conductive heat transfer across the solid regions are solved coupled with the fluid dynamic equations. Second order schemes are employed for the spatial discretization. Turbulence is modeled with a Chen $k - \epsilon$, using a two-layer algorithm in the near wall region.

B. Computational grid

The IDEAS CAD and mesh generator [8] have been employed to create a parametric mixed structured/unstructured mesh. Unstructured meshes are used in zones with irregular geometry and whose shape varies with the values of the parameters (like the funnel zone on the left of Fig. 4). The fluid regions near the walls are meshed with structured grids, easier to handle and more suitable for the application of the turbulent near-wall algorithms (see Fig. 4).

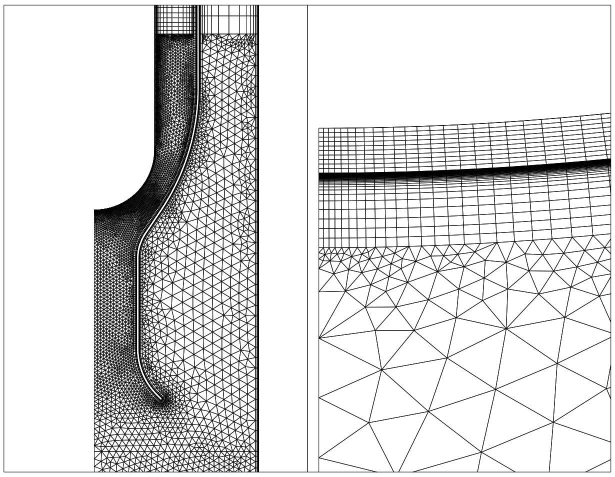

Figure 4: The non-structured mesh in the funnel zone (on the left) and the structured mesh in the window and in the near-wall region.

Structured meshes are also used for the discretization of the solids. The flow guide is split into three regions along its thickness to allow the simulation of the Zirconia insulation. In order to make possible using meshes with different coarseness in the rising and downcoming sides, the flow guide is discretized with a non-conform mesh. The total number of cells is about 25000 (it varies while changing the parameters in the non structured zones). The discretization is very accurate in the funnel zone, especially next to the window stagnation point. Cells with high aspect ratio are used in the rising and downcoming duct, where the flow is supposed to be regular.

[d]For example the curvature radius of the stretch of flow guide that defines the connector can be fixed.

C. The FLUKA Heat Source Distribution

The interactions between the proton beam and the window and coolant materials are simulated with the FLUKA code [9]. The result of this calculation is a volumetric heat source distribution (in $W/cm^3/mA$) that must be applied in the TFD simulation. The heat source distribution in the window is given by an analytical curve as a function of the distance from the beam axis. The distribution of the heat generated in the Pb-Bi by the spallation process is given in form of table on a discretization grid as a function of the position with respect to the window center. The table file is read by Star-CD and interpolated on the computational grid. The resulting heat source distributions on the coolant and on the window are shown in Fig. 5. The heat generated inside the materials of the funnel flow guide is calculated by applying the distribution for the Pb-Bi multiplied by the ratio of the density of the flow guide material (HT-9 or ZrO_2) and the density of the Pb-Bi.

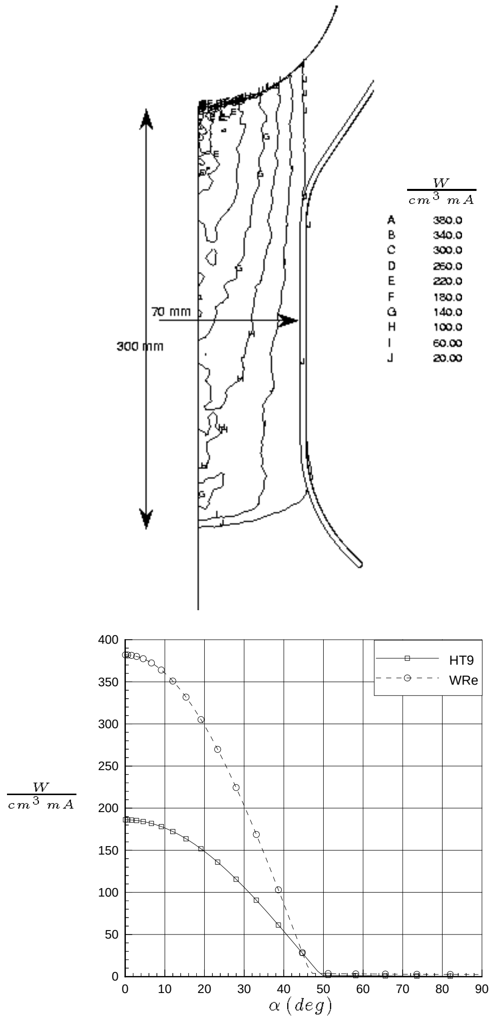

Figure 5: FLUKA heat source distribution in the Pb-Bi (on the top, in $W/m^3/mA$) and in the window.

D. Structural Analysis

The same grid used for the TFD simulation was employed for the finite element structural simulation of the beam pipe - window system. The nodes belonging to the surface on the top of beam pipe have been constrained with a slider that restrains the displacements normal to the plane of that surface. The choice of this constraint is not relevant because its effects are quickly damped in the very vicinity of the constraint itself. The temperature field calculated by Star-CD is assigned to the elements of the model and the Pb-Bi hydrostatic pressure distribution is applied onto the external surface.

IV. RESULTS

All the calculation have been done with heat exchanger outlet temperature set to 180 $°C$. The graphs of the window temperature and stresses distribution are obtained plotting the values of the first row of cells next to the external (window - coolant interface) and internal (window - void interface) sides of the window as a function of the angle α between the target axis and a radius of the window circumference.

B. Comparison between the W-Re and the HT-9 Window

1. TFD analysis. A first set of calculations was done with a beam intensity of 2 mA in order to compare the behaviour of W-Re and HT-9 as window materials. Concerning the thermo-fluid-dynamic simulation the only difference between the two cases is the heat produced in the window (in the W-Re it is nearly twice as that in the HT-9; see Tab. 1) and the thermal characteristics of the two materials (in particular the thermal conductivity of W-Re is nearly four times that of HT-9).

material	$\dot{Q}_w$	$\overline{T}_w$	$T_{w,max}$	$T_{w,min}$	vms_{max}
W-Re	13.4	270	322	251	334
HT-9	7.2	267	319	251	49.8

Table 1: results of the window materials analysis ($[\dot{Q}_w] = KW$, $[T] =° C$, $[vms] = MPa$).

The cooling flow is not significantly influenced by the difference in the heat production in the window, so it has the same characteristics for both cases ($\dot{m} \simeq 139\,Kg/s$)[e].

[e] As shown later, the features of the cooling flow have negligible effects on the window stress field, so that the results presented

Fig. 6 shows the temperature distribution in the window for the two cases. Radial temperature gradients can be observed in the window region crossed by the proton beam (the proton beam is a circular spot of 150 mm, so it strikes the window up to an angle of 48.6 degrees). These gradients are necessary to transfer the heat produced inside the window to the external surface and hence to the coolant, and depend almost exclusively on the characteristics of the proton beam and on the thermal characteristics of the window material. In fact the conductive heat flux in the tangential direction, which depends on the tangential temperature gradients and therefore could be influenced by the cooling flow features, is much smaller than the radial flux in the region interested by the proton beam. In Fig. 6 we observe a smaller temperature difference in the radial direction in the case of W-Re (whose conductivity is higher), in spite of a higher heat generation. However, since the convective heat exchange coefficient is almost the same in both cases (as said above the cooling flow has the same characteristics in both cases), a higher temperature in the external surface is needed to transfer to the coolant the greater heat production in the W-Re window. The result of these two effects is a slightly greater maximum temperature in the W-Re window.

2. Structural analysis. As shown in Fig. 7, in the case of the W-Re window-HT9 pipe in the surroundings of the joint there is a peak of the stresses comparable with the yielding stress value of the steel (see also Tab. 1 where the maximum Von Mises Stress vms_{max} is reported). The difference between the thermal expansion coefficients amplifies the bending effects due to the shearing forces involved in the cooperation of the cylinder with the hemispherical end. The stress

here are quite general.

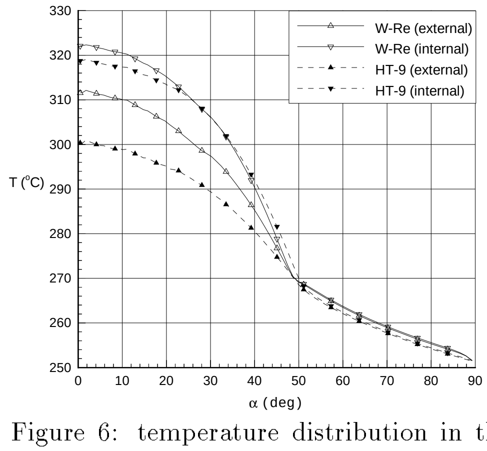

Figure 6: temperature distribution in the W-Re and HT-9 windows.

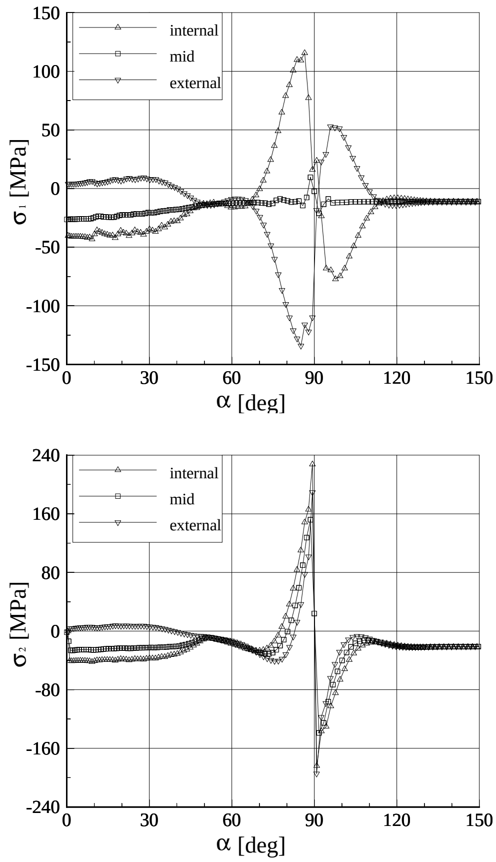

Figure 7: meridional (σ_1) and hoop (σ_2) stress distributions at the external-internal-middle fibres in the W-Re window.

distribution in the rest of the window is quite similar for both cases. It can be seen (Fig. 8) that the thinner part of the window, which is also the most loaded, undergoes strong bending moments depending basically on the temperature gradient along the thickness. The curves representing the stress components at the internal surface present a series of peaks in the proximity of the window center. This phenomena, from an analytical point of view, could be explained by a superposition of oscillatory stress fields generated by the temperature gradient variation.

C. Optimization of the Funnel and the Flow Guide Diameters

As previously explained, the two most significant parameters for the target performances are the funnel diameter D_f (which regulates the velocity of the coolant in the funnel, and then the coolant temperature distribution through the spallation region, and the heat exchange coefficient of the window) and the flow guide diameter D_{fg} (which acts on the pressure losses distribution in the coolant circuit and then on the mass flow rate). A parametric study of these two quantities is reported below.

The global set-up of the system is shown in Tab.

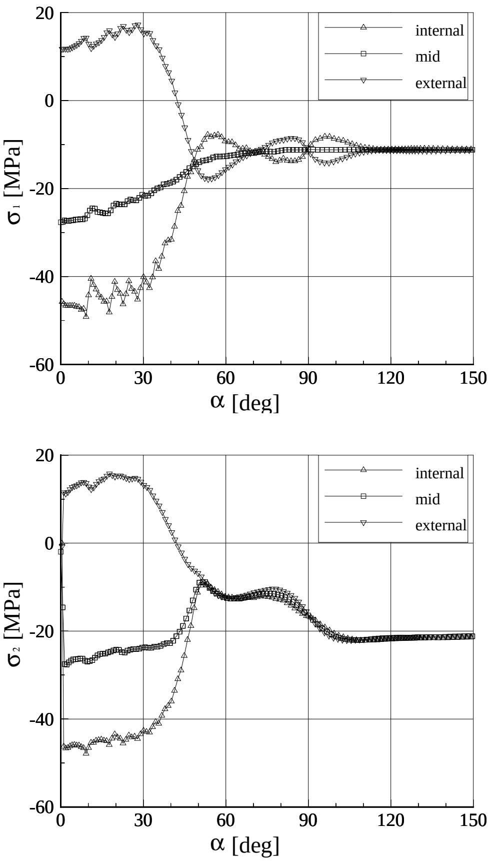

Figure 8: meridional (σ_1) and hoop (σ_2) stress distributions at the external-internal-middle fibres in the HT-9 window.

2. Nine calculations were performed with the funnel diameter at 140, 160 and 180 mm and the flow guide diameter at 284, 400 and 460 mm. The minimum dimension of D_f was chosen 10 mm smaller than the proton beam diameter in correspondence of the FLUKA 25 $MW/m^3/mA$ power isoline (see Fig. 5).

quantity	value
H	$\simeq 6\ m$
D_c	$0.68\,m$
I_{beam}	$2\,mA$
Window material	HT-9

Table 2: model characteristics for the D_f - D_{fg} parametric analysis.

Fig. 9 shows the dependence of the mass flow rate (i.e. of the pressure losses of the circuit) on the two parameters. For small values of D_{fg} the pressure losses distributed in the rising column are much more important than the local losses in the inducer, the funnel and the connector, especially for larger values of D_f, so the mass flow rate is strongly dependent on D_{fg}. It can be seen how a maximum mass flow rate is reached for $D_{fg} = 400\,mm$ [f]. With this configuration the pressure

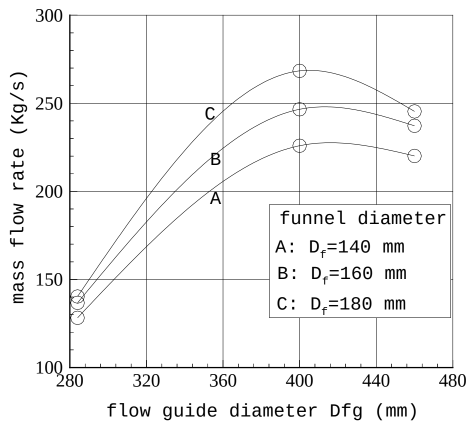

Figure 9: mass flow rate as a function of the flow guide diameter for different funnel diameters (the data points are interpolated with splines).

losses in the connector are the most important and the funnel diameter has a stronger influence on the mass flow rate. However, although the mass flow rate decreases with D_f, the velocity in the funnel grows leading to a lower heating of the flow cooling the window and hence to lower temperatures in the window itself, as shown in figure 10.

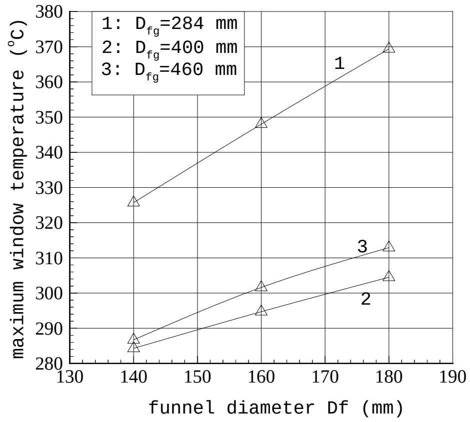

Figure 10: maximum window temperature as a function of the funnel diameter for different flow guide diameters.

D. Dependence of the Window Temperature and Stresses on the Mass Flow Rate

1. TFD analysis. Starting from the model described in the previous section with the funnel diameter set to 140 mm (which gave the best results in the optimization study), the upper part of the circuit has been cut in the section corresponding to the outlet of the

[f] Two more calculations with $D_f = 140\,mm$ and D_{fg} at 380 and 430 mm were done in order to check the position of the maximum mass flow rate.

heat exchanger, and inlet and outlet boundary conditions have been imposed in the downcoming and rising columns respectively. The mass flow rate is imposed and hence it is no more a result of the chimney effect. The inlet temperature (i.e. the temperature of the fluid at the outlet of the heat exchanger) is 180 $°C$ (as in the previous calculations) while the current intensity of the proton beam was increased from 2 to 6 mA, so that the power released in the window and in the coolant is three times higher with respect to the previous simulations. Five calculations were performed with the mass flow rate varying from 150 to 250 Kg/s.

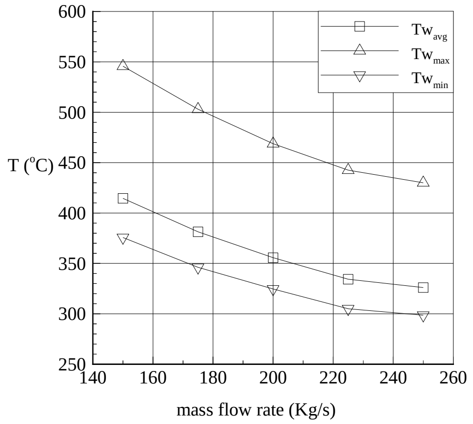

Figure 11: Window temperatures as a function of the mass flow rate.

Fig. 11 shows the variation of the window temperatures (mean, maximum and minimum) as a function of the mass flow rate. Considering that the temperature application range suggested for the HT-9 steel is between 300 and 500 $°C$ [10] a mass flow rate of 200 Kg/s seems to give the better results.

1. Structural analysis. The structural analysis has been performed for the cases with mass flow rate 150, 200 and 250 Kg/s in order to ascertain the effect of changing the characteristics of the cooling flow on the stress intensity and distribution in the window. As shown in Fig. 12,

in spite of a mean temperature variation of order 100$°C$ and a sensible variation in the longitudinal temperature distribution, the stress field is substantially identical in all the three cases. This means that the stresses produced by the transversal temperature gradients, which depends almost exclusively on the beam characteristics (as previously explained), are much greater than those generated by the mean temperature increase or by the longitudinal temperature gradients. In conclusion the stress field in the window, calculated with a linear (elastic) model, is not influenced by changing the characteristics of the cooling flow.

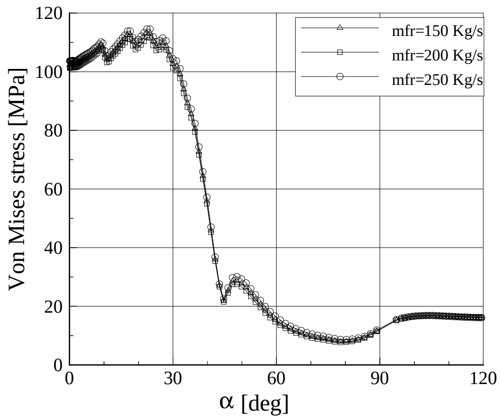

Figure 12: Von Mises stress distribution in the window external fibres for different mass flow rates.

E. Dependence of the Window Temperature and Stresses on the Beam Intensity

The system response to the variation of the proton beam intensity is analysed. The full system in natural convection is considered, so that the mass flow rate is a result of the simulation. The model dimensions are those described in section D. Five cases with the beam intensity ranging from 2 to 6 mA have been considered. Fig. 13 shows the variation of the maximum temperature and Von Mises stress in the window with the beam intensity.

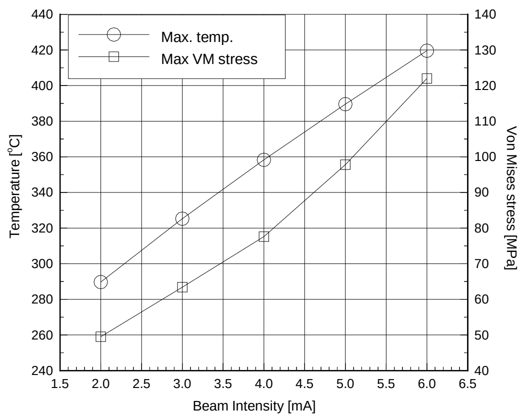

Figure 13: Maximum Temperature and Von Mises stress in the window as a function of the beam intensity.

V. CONCLUSIONS

Extensive numerical calculations have been performed to study the thermo-fluid-dynamics and the structural stress of the window-type beam target. The results show that the HT-9 steel can be employed as window material with a proton beam energy of 600

MeV and a beam current from 2 to 6 mA, which is the operation intensity range foreseen for the Energy Amplifier prototype. Infact it has been shown that the operational are below the limit suggested for the HT-9 steel [10], with the maximum stress well below the minimum yield strength of this material.

With the target height set to 6 m, natural circulation is sufficient to pump the coolant mass flow rate necessary to remove the heat generated in the Pb-Bi by the spallation process and in the window by the ionization losses. Finally, the response to different mass flow rates and different beam intensities has been studied, making possible the analysis of the behaviour of the system in different operating conditions,

References

[1] C. Rubbia et al., "Conceptual Design of a Fast Neutron Operated High Power Energy Amplifier", CERN/AT/95-44 (ET), Geneva, September 1995.

[2] STAR-CD, *Version 3.0 Manual*, Computational Dynamics, London, 1996.

[3] MSC/Nastran, *Reference Manual (Version 68)*, 1994, MacNeal-Schwendler Corporation.

[4] Proceedings of the Meetings ICANS-XIII and ESS-PM4, edited by G. Bauer and R. Bercher, PSI proceedings 95-02, November 1995.

[5] Proceedings of the *International Workshop on the Technology and Thermal Hydraulics of Heavy Liquid Metals*, B.R. Appleton, G.S. Bauer, Schruns, Austria, March 25-28 1996.

[6] S. Buono, C. Rubbia, "A Comparison of Different Materials for the Beam Window of the Energy Amplifier", CERN/ET Internal Note 96-26, August 1996.

[7] S. Buono, C. Rubbia, "A Tungsten-Rhenium Alloy as a Beam window Material for the Energy Amplifier", CERN/ET Internal Note 96-24, July 1996.

[8] I-DEAS Master series, *Reference Manual*, 1996, SDRC (Structural Dynamics Research Corporation).

[9] A. Fasso' et al., *FLUKA 92*, Proc. of the Workshop on Simulating Accelerator Radiation Environments, Santa Fe,11-15 January 1993.

[10] Y. Dai, "Martensitic/ferritic Steels as Container Materials for Liquid Mercury Target of ESS", *International Workshop on the Technology and thermal hydraulics of Heavy Liquid Metals*, Schruns (Austria), March 1996.